XLVI CILAMCE
VITÓRIA - ES - BRAZIL - 2025
XLVI IBERO-LATIN AMERICAN CONGRESS ON COMPUTATIONAL METHODS IN ENGINEERING

Review of resistance prediction methods for double-skin composite columns

Lívia C. L. Sousa[1], Jerfson M. Lima[1], Jorge D. B. Rocha[2], Jonathas I. F. De Oliveira[1], Nicolas S. F. Dias[1], Bruna G. Almeida[1]

[1]*Federal University of Ceará, Russas Campus*
R. Felipe Santiago, 411 – University City, Russas – CE, 62900-000, Brazil
liacristina2002@alu.ufc.br, jerfson.lima@ufc.br, jbonillarocha@gmail.com, steniodias@alu.ufc.br, brunagenu@alu.ufc.br
[2]*University of Brasília, Darcy Ribeiro University Campus*
Asa Norte, Brasília – DF, 70910-900, Brazil
jbonillarocha@gmail.com

Abstract. Derived from CFST (Concrete-Filled Steel Tube) columns, CFDST (Concrete-Filled Double Skin Tubular) columns are composite elements composed of two concentric steel tubes, an inner and an outer, with concrete filled in the annular space. Typically, carbon steel is used for the inner tube, while the outer tube may be made of carbon or stainless steel. These columns offer key advantages such as improved concrete confinement, high axial load capacity, reduced self-weight, enhanced local buckling resistance, and increased ductility. The use of stainless steel externally also improves durability, resistance to environmental agents, aesthetics, and construction ease. Owing to these benefits, research into their structural behavior has increased. Despite extensive experimental and numerical studies using the Finite Element Method, no specific design standard exists for CFDST columns with stainless steel outer tubes, prompting the proposal of new predictive models. This work reviews the main approaches for estimating axial capacity, comparing equations from ACI 318: 2011, AISC 360: 2016, GB 50936: 2014, Eurocode 4: 2004, and those proposed by authors in the literature. An experimental database from the literature comprising 56 CFDST columns, including both short and slender columns, was used to verify the accuracy of the prediction methods. For short CFDST columns, among the standards analyzed in this study, the formulations presented in Eurocode 4:2004 proved to be more satisfactory. Among the formulations from the literature, the model proposed by Han et al. (2018) proved to be the most efficient. However, for slender CFDST columns, no standard or formulation from the literature showed good efficiency.

Keywords: steel-concrete composite columns, CFDST columns, double-skin columns, offshore structures.

1 Introduction

Due to the constant search for ways to preserve the environment, particularly methods to reduce carbon dioxide (CO_2) emissions, alongside concerns related to electricity generation, the demand for renewable energy sources has significantly increased in recent decades. However, advantages such as higher wind speed and stability, along with reduced noise and visual impact, have made offshore wind energy a viable alternative to onshore wind energy. Amid the ambition for projects and technologies capable of neutralizing greenhouse gas emissions, structural engineering is increasingly challenged. The main disadvantage of wind farm installation lies in its construction and installation costs, which rise with sea depth, therefore, increasingly slender structures are required. Moreover, dynamic forces and exposure to the marine environment must be taken into account, as many structural accidents related to wind farms highlight the need to carefully assess the load-bearing capacity and durability of structural components (Lima et al., 2024 [1]).

Given the above, CFDST (Concrete-Filled Double Skin Tubular) columns have proven to be a viable option

for the construction of offshore wind towers, as well as for other types of structures such as offshore platforms, electrical transmission towers, and tall, mega-tall, or super-tall buildings. CFDST columns (Fig. 1), also known as double-skin columns, are composite structures made of two steel tubes filled with concrete between them that, in addition to offering high load-bearing capacity and reduced self-weight, also provide greater protection against external agents due to the outer steel tube (Gonçalves et al., 2024 [2]).

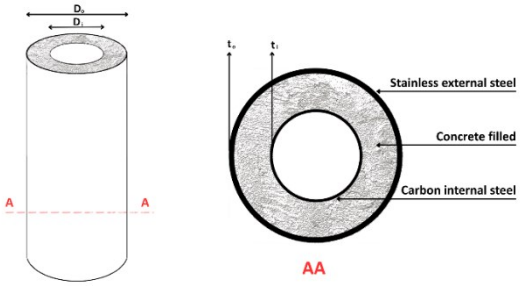

Figure 1 – CFDST columns

The American Concrete Institute (ACI) 318: 2011 [3] and American Institute of Steel Construction (AISC) 360: 2016 [4] provide design methods for CFST columns, however, they do not provide formulations for calculating the load-bearing capacity of CFDST columns. In contrast, the National Standard of the People's Republic of China (GB) 50936: 2014 [5] and Eurocode 4: 2004 [6] standards offer equations for designing CFDST columns, but these equations consider only carbon steel tubes. The lack of methods for designing CFDST columns has encouraged researchers to develop new formulations. Uenaka et al.'s (2010) [7] equation was only proposed for carbon steel tube, for cross-sections with the D_i/D_o ratio limited to a $0.2 < D_i/D_o < 0.7$ range. Hassanein et al.'s (2013) [8] design proposal was developed for carbon steel inner tube, stainless steel outer tube and outer steel tube slenderness of $D_o/t_{so} < 59$, a concrete compressive strength varying from 40 to 120 MPa and limits of strain hardening effects for both steel tubes, i.e., 1.2 for the stainless steel tube and between 0.9 and 1.1 for the carbon steel tube. Han et al.'s (2018) [9] method was developed for carbon steel inner tubes, stainless steel outer tubes and a hollow ratio (x) varying from 0.5 to 0.75. Castanheira (2021) [10] developed an N-M interaction diagram using MATLAB software, and was based on a rigid-plastic material analysis assuming a rectangular stress block distribution.

In this context, the present study aims to compile the aforementioned design methods and evaluate their respective accuracies. To this end, the load-bearing capacity of 56 experimental columns was calculated using the formulations of each method and compared with the experimental ultimate load.

2 Design Methods

The formulations for calculating the ultimate load according to the standards and the methods proposed in the literature are shown in Tables 1 and 2, respectively.

Table 1 – Standards

Design Codes	Design equations
ACI 318 [3]	$\boldsymbol{P_{n,ACI} = A_{so}f_{so} + A_{si}f_{syi} + 0.85A_cf_c}$, *only for short columns*
AISC 360 [4]	$\boldsymbol{P_{n,AISC} = \begin{cases} P_{no}\left(0.658^{\frac{P_{no}}{P_e}}\right), when\ \frac{P_{no}}{P_e} \leq 2.25 \\ 0.877P_e \quad , when\ \frac{P_{no}}{P_e} > 2.25 \end{cases}}$

$$P_{no} = \begin{cases} P_p = A_{so}f_{yo} + 0.95A_cf_c + A_{si}f_{yi}\ , for\ compact\ sections\ (\frac{D_o}{t_o} < \lambda_p) \\ P_p - \frac{P_p - P_y}{(\lambda_r - \lambda_p)^2}(\lambda - \lambda_p)^2, for\ noncompact\ sections\ (\lambda_p \le \frac{D_o}{t_o} \le \lambda_r) \\ A_{so}F_{cr} + 0.7A_cf_c + A_{si}f_{yi}\ , for\ slender\ sections\ (\lambda_r \le \frac{D_o}{t_o} \le \lambda_{máx}) \end{cases}$$

$$P_e = \frac{\pi^2(EI)_e}{(KL)^2}$$

$$P_y = f_{yo}A_{so} + 0.7f_cA_c + f_{yi}A_{si}$$

$$F_{cr} = \frac{0.72f_{yo}}{\left[\left(\frac{D_o}{t_o}\right)\frac{f_{yo}}{E_s}\right]^{0.2}}$$

GB 50936 [5]

$$\boldsymbol{P_{n,GB} = \phi\left[(A_{so} + A_c)f_{osc} + A_{si}f_{yi}\right]}$$

$$\phi = \frac{1}{2\bar{\lambda}_{osc}^{\ 2}}\left[\bar{\lambda}_{osc}^{\ 2} + \left(1 + 0.25\bar{\lambda}_{osc}\right) - \sqrt{\left(\bar{\lambda}_{osc}^{\ 2} + \left(1 + 0.25\bar{\lambda}_{osc}\right)\right)^2 - 4\bar{\lambda}_{osc}^{\ 2}}\right]$$

$$\bar{\lambda}_{osc} = \left(\frac{\lambda}{\pi}\right)\sqrt{\frac{f_{osc}}{E_{osc}}}$$

$$f_{osc} = (1.212 + B\xi + C\xi^2)f_c$$

$$E_{osc} = \frac{E_{so}I_{so} + E_{si}I_{si} + E_cI_c}{I_{osc}}$$

$$\xi = \frac{A_{so}f_{so}}{A_cf_c} = \alpha\frac{f_{yo}}{f_c}$$

Eurocode 4 [6]

$$\boldsymbol{P_{n,EC4} = \eta_aA_{so}f_{yo} + A_cf_c\left[1 + \eta_c\left(\frac{t_{so}}{D}\right)\left(\frac{f_{yo}}{f_c}\right)\right] + A_{si}f_{yi}}$$

$$\eta_c = \eta_{c0}\left(1 - \frac{10e}{D}\right)\ \ but\ 0 < \frac{e}{D} \le 1.0$$

$$\eta_a = \eta_{a0} + (1 - \eta_{a0})\left(\frac{10e}{D}\right)\quad but\ 0 < \frac{e}{D} \le 1.0$$

$$\eta_{c0} = 4.9 - 18.5\bar{\lambda} + 17\bar{\lambda}^2\ \ but \ge 0$$

$$\eta_{a0} = 0.25(3 + 2\bar{\lambda})\ but \le 1.0$$

$$\bar{\lambda} = \sqrt{\frac{P_{pl,Rd}}{P_{cr}}}$$

$$P_{pl,Rd} = A_{so}f_{so} + \alpha_{cc}A_cf_c + A_{si}f_{yi}$$

$$P_{cr} = \frac{\pi^2(EI)_{eff}}{kL^2}$$

$$(EI)_{eff} = E_{so}I_{so} + K_eE_cI_c + E_{si}I_{si}$$

*In which $\boldsymbol{A_{so}}$, $\boldsymbol{A_c}$, $\boldsymbol{A_{si}}$, $\boldsymbol{f_{so}}$, $\boldsymbol{f_c}$, $\boldsymbol{f_{yi}}$, $\boldsymbol{E_{so}I_{so}}$, $\boldsymbol{E_cI_c}$ and $\boldsymbol{E_{si}I_{si}}$ are the parameters already used by previous authors and refer to the area, resistance and rigidity of the section components; $\boldsymbol{P_{no}}$ is the nominal axial compressive resistance; $\boldsymbol{P_e}$ is the elastic critical buckling load; $\boldsymbol{(EI)_e}$ is the effective stiffness; $\boldsymbol{KL}$ is the effective length; $\boldsymbol{\lambda}$ is the slenderness ratio of the outer tube ($\frac{D_o}{t_o}$); the values of $\boldsymbol{\lambda_p}$, $\boldsymbol{\lambda_r}$ and $\boldsymbol{\lambda_{máx}}$ are shown in Table I 1.1a of the AISC 360:2016 [4]; Fcr is the critical buckling stress; $\boldsymbol{\bar{\lambda}_{osc}}$ is the non-dimensional slenderness; B = 0.176*fyo/213 + 0.974 and C = -0.104*fc/14.4 +0.031 are the algebraic factors; $\boldsymbol{E_{so}}$ is the composite bending modulus; $\boldsymbol{(EI)_{eff}}$ is the composite cross section effective flexural stiffness; $\boldsymbol{K_e}$ is the correction factor with a value of 0.6; $\boldsymbol{P_{pl,Rd}}$ is the compressive plastic resistance; and $\boldsymbol{P_{cr}}$ is the elastic critical normal force for relevant buckling mode.

Table 2 – Formulations of literature

Design Codes	Design equations
Uenaka et al. (2010) [7]	$\boldsymbol{P_{n,Uenaka} = (1 + \eta_{CFDST})A_{so}f_{yo} + A_cf_c + A_{si}f_{yi} \quad but\ 0.2 < \frac{d}{D} < 0.7}$ $\eta_{CFDST} = 1.86 - 2.59\left(\frac{d}{D}\right)$
Hassanein et al. (2013) [8]	$\boldsymbol{P_{n,Hassanein} = \gamma_{so}A_{so}f_{yo} + (\gamma_cf_c + 4.1f_1)A_c + \gamma_{si}A_{si}f_{yi}}$ $\gamma_{so} = 1.62\left(\frac{D}{t_{so}}\right)^{-0.1} \quad but\ \gamma_{so} \leq 1.2$ $\gamma_{si} = 1.458\left(\frac{d}{t_{si}}\right)^{-0.1} \quad but\ 0.9 \leq \gamma_{si} \leq 1.1$ $\gamma_c = 1.85D_c^{-0.135} \quad but\ 0.85 \leq \gamma_c \leq 1.0$ $D_c = D - 2t_{so}$ $f_1 = \begin{cases} 0.7(v_o - v_s)\frac{2t_{so}}{D - 2t_{so}}f_{yo} & for\ \frac{D}{t_{so}} \leq 47 \\ \left(0.006241 - \frac{0.0000357D}{t_{so}}\right)f_{yo} & for\ 47 < \frac{D}{t_{so}} \leq 150 \end{cases}$ $v_o = 0.2312 + 0.3582v_o' - 0.1524\left(\frac{f_c}{f_{yo}}\right) + 4.843v_o'\left(\frac{f_c}{f_{yo}}\right) - 9.169\left(\frac{f_c}{f_{yo}}\right)^2$ $v_o' = 0.881 \times 10^{-6}\left(\frac{D}{t_{so}}\right)^3 - 2.58 \times 10^{-4}\left(\frac{D}{t_{so}}\right)^2 + 1.953 \times 10^{-2}\left(\frac{D}{t_{so}}\right) + 0.4011$
Han et al. (2018) [9]	$\boldsymbol{P_{n,Han} = \phi(P_{i,u} + P_{osc,u})}$ $\phi \begin{cases} 1 \quad for\ \lambda \leq \lambda_0 \\ a\lambda^2 + b\lambda + c \quad for\ \lambda_o < \lambda \leq \lambda_p \\ \frac{d(-0.23\chi^2 + 1)}{(\lambda + 35)^2} \quad for\ \lambda > \lambda_p \end{cases}$ $P_{i,u} = A_{si}f_{yi}$ $P_{osc,u} = A_{osc}f_{osc}$ $A_{osc} = A_c + A_{so}$

$$f_{osc} = C_1\chi^2 f_{yo} + C_2(1.14 + 1.02\xi)f_c$$

$$C_1 = \frac{\alpha}{(1+\alpha)}$$

$$C_2 = \frac{1+\alpha_n}{1+\alpha}$$

$$\chi = \frac{d}{D - 2t_{so}}$$

$$\xi = \frac{A_{so}f_{yo}}{A_{ce}f_c}$$

$$A_{ce} = \frac{\pi(D-2t_{so})^2}{4}$$

	$\boldsymbol{P_{n,Castanheira} = f_{yo}\pi(R^2 - R_c^2) + f_{cc}\pi(R_c^2 - r^2) + f_{yi}\pi\left(r^2 - r_{(i-t_{si})}^2\right)}$
Castanheira (2021) [10]	$\frac{f_{cc}}{f_c} = 0.08 \times \eta + 0.06 \;\; since \; \frac{f_{cc}}{f_c} \geq 1$ $\eta = 1.0 \;\; for \; f_c \leq 50MPa$ $\eta = 1.0 - \frac{f_c - 50}{200} \quad for \; 50 < f_c \leq 90MPa$

∗ $\boldsymbol{f_1}$ is the lateral confining pressure; $\boldsymbol{v_o}$ is the Poisson's coefficient of the steel tube with the concrete infill; $\boldsymbol{v_s}$ is the Poisson's coefficient of the steel tube without the concrete infill and at the maximum strength point, with a value of the 0.5; $\boldsymbol{a}$, $\boldsymbol{b}$, $\boldsymbol{c}$ and $\boldsymbol{d}$ are the parameters related to the buckling reduction coefficient presents in Han et al. (2018) [10]; $\boldsymbol{\lambda_0}$ and $\boldsymbol{\lambda_p}$ are slenderness limit values; $\boldsymbol{\xi}$ is the confinement factor; $\boldsymbol{\alpha}$ is the ratio of the outer stainless tube area $\boldsymbol{A_{so}}$ to the concrete cross-section area $\boldsymbol{A_c}$; $\boldsymbol{\alpha_n}$ is the ratio of $\boldsymbol{A_{so}}$ to $\boldsymbol{A_{ce}}$; $\boldsymbol{A_{ce}}$ is na equivalent cross-section area of the sandwiched concrete; $\boldsymbol{R}$, $\boldsymbol{R_c}$ and $\boldsymbol{r}$ are the radius of the outer steel tube, the infilled concrete and the inner steel tube under compression.

3 Verification of the accuracy of the double-skin columns resistance prediction

The load-bearing capacity ($P_{n,exp}$) of 56 experimental tests was evaluated using these formulations and compared with the corresponding experimental capacity. The database was composed of the experimental tests by Tao et al. (2004) [11]; Li and Cai (2012) [12]; Uenaka et al. (2010) [7]; Li and Cai (2019) [13] and Ekmekyapar and Hasan (2019) [14]; and consists mostly of short double-skin columns. However, it also includes a proportion of slender columns in order to assess the accuracy of the formulations for both column configurations. The criterion adopted for the classification of the columns was the ratio between the height (L) and the external diameter (D). Columns with L/D ≤ 3 were considered short, whereas those with L/D > 3 were classified as slender. This classification is common in experimental investigations. The database consists of columns with internal carbon steel and external steel, either carbon steel or stainless steel, and the characteristics of the experimental columns are presented in Table 3. To evaluate the performance of the methods, the values of the Coefficient of Determination (R^2), Root Mean Square Error (RMSE), and Mean Absolute Percentage Error (MAPE) will be assessed, as described below. Where E_i and P_i represent the experimental and predicted values of the shear capacity P_n, respectively; n is the total number of specimens.

Table 3 – Summary of statistical attributes of database

Parameter	**Mean**	**Min**	**Median**	**Max**
L (mm)	815.89	342.00	569.70	3457.00
D_o (mm)	187.69	114.00	189.45	356.00
t_o (mm)	4.13	0.90	5.05	6.80
f_{yo} (MPa)	347.77	221.00	342.00	618.00
D_i (mm)	82.63	33.50	59.85	231.00
t_i (mm)	3.39	0.90	3.20	8.00
f_{yi} (MPa)	339.88	221.00	342.00	397.00
f_c (MPa)	41.24	18.70	37.50	138.00
D_o/t_o	50.50	36.36	41.76	126.67
D_i/t_i	24.01	15.60	19.80	37.76
D_o/D_i	2.56	1.54	2.72	3.40
$P_{n,exp}$ (kN)	2324.27	378.00	2461.00	7242.00

$$R^2 = \left(\frac{\sum\left((P_i - \overline{P_i}) * (E_i - \overline{E_i})\right)}{\sqrt{\sum(P_i - \overline{P_i})^2 * \sum(E_i - \overline{E_i})^2}} \right)^2 \quad (1)$$

$$RMSE = \sqrt{\frac{\sum_{i=1}^{n}(E_i - P_i)}{n}} \quad (2)$$

$$MAPE = \frac{\sum_{i=1}^{n}\left(\frac{E_i - P_i}{E_i}\right)}{n} \quad (3)$$

Fig. 2 presents an overview of the accuracy of the design methods addressed in this work, showing graphs of experimental axial load versus calculated axial load for each formulation. Data points located above the red line correspond to experimental tests in which the design method proved to be conservative, whereas points below the line indicate a lack of safety in the column's double-skin load-bearing capacity equation. Regarding design codes, Fig. 2(a) shows that the ACI 318: 2011 [3] is the most conservative, in contrast to the Eurocode 4:2004 [6], shown in Fig. 2(d), whose data align more closely with the red line. As for formulations of literature, the method proposed by Uenaka et al. (2010) [7], presented in Fig. 2(e), proves to be non-conservative and exhibits poor agreement with the red line. Conversely, the formulation by Han et al. (2018) [9], shown in Fig. 2(g), demonstrates acceptable alignment.

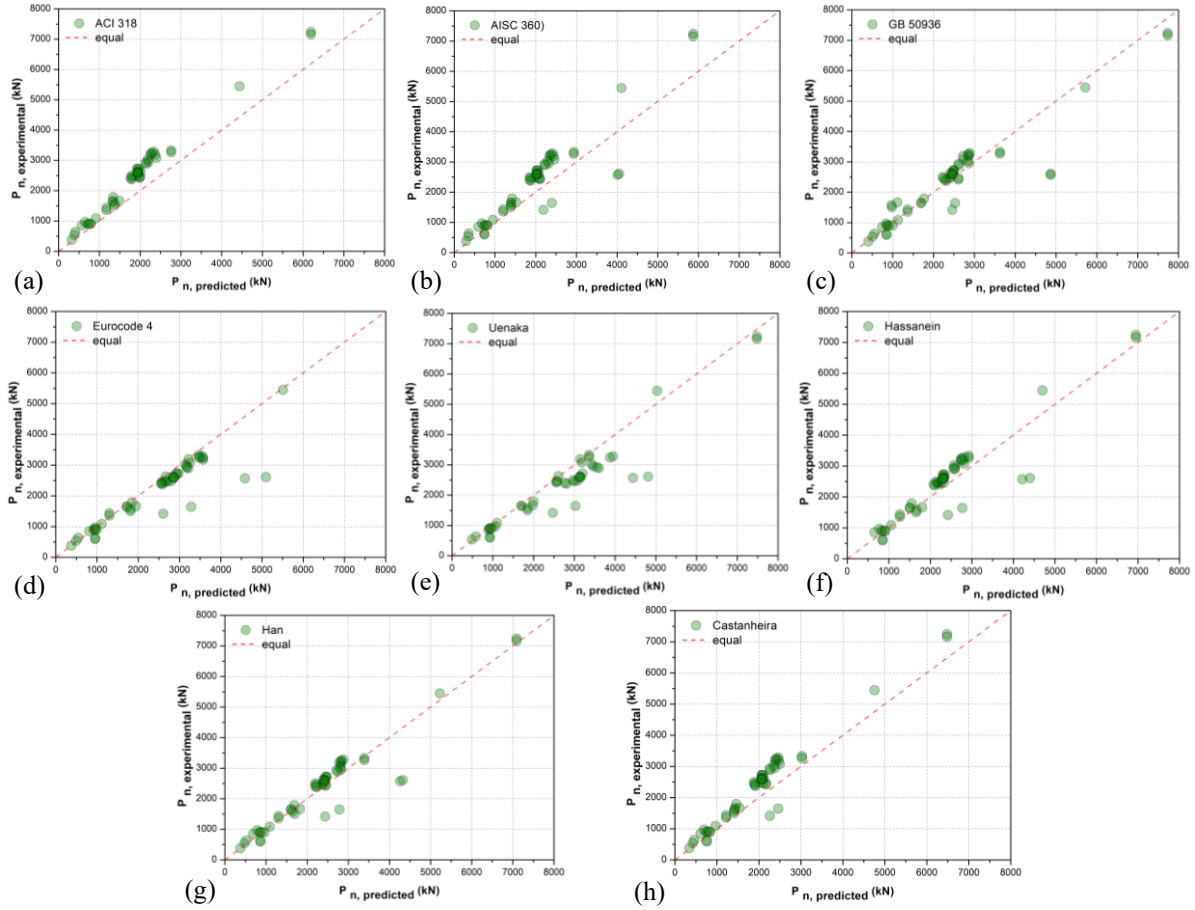

Figure 2 – Prediction performance of 6 empirical equations: (a) ACI; (b) AISC; (c) GB; (d) Eurocode 4; (e) Uenaka et al. (2010); (f) Hassanein et al. (2013); (g) Han et al. (2018); (h) Castanheira (2021).

Tables 4 and 5 present the performance metrics for short and slender columns, respectively, for each of the double-skin column design methods analyzed in this study. In Table 4, the values for ACI 318:2011 [3] were not included, as the equation is only valid for short columns. For short columns, on average, ACI 318: 2011 [3] proved to be the most conservative method, oversizing the double-skin columns by 30.3%. Despite this, AISC 360: 2016 [4] showed the highest ratio between the experimental and calculated axial loads, with a value of 77.8%. The least conservative method, on average, was that of Uenaka et al. (2010) [7], underestimating the column strength by 8.5%, and also presenting the lowest ratio between experimental and calculated axial loads, at 19.7%. On average, the formulation with the best ratio of $P_{n,exp}/P_{n,pred}$ was the one proposed by Han et al. (2018) [9], which also showed a satisfactory R^2 value of 0.990, the lowest RMSE value of 196.297 kN, and an acceptable MAPE of 7.4%.

For slender columns, on average, the method proposed by Castanheira (2021) [10] showed the best $P_{n,exp}/P_{n,pred}$ ratio, however, the equation presents R^2, RMSE, and MAPE values of 0.46, 595.86kN, and 40%, respectively, indicating a poor fit of the formulation. Eurocode 4 [6] proved to be the least conservative, presenting an average $P_{n,exp}/P_{n,pred}$ ratio of 56% and a minimum ratio of 50%. Although most methods showed satisfactory R^2 values, except for the one proposed by Castanheira (2021) [10], all RMSE and MAPE values were considerable. This is due to the low number of slender columns in the database.

Table 4 – Performance metrics of design methods for shorts columns

Statistical parameters	ACI	AISC	GB	EC4	Uenaka	Hassanein	Han	Castanheira
$P_{n,exp}/ P_{n,pred}$ – Mean	1.303	1.271	1.074	0.948	0.915	1.114	1.066	1.222
$P_{n,exp}/ P_{n,pred}$ – Maximum value	1.557	1.778	1.628	1.162	1.113	1.304	1.242	1.393
$P_{n,exp}/ P_{n,pred}$ – Minimum value	1.107	1.082	0.899	0.830	0.803	0.911	0.885	1.069
$P_{n,exp}/ P_{n,pred}$ – Standard deviation	0.107	0.124	0.143	0.063	0.083	0.076	0.074	0.093
$P_{n,exp}/ P_{n,pred}$ – Coefficient of variation (%)	8.220	9.790	13.359	6.617	9.107	6.798	6.962	7.611
R^2	0.981	0.986	0.976	0.993	0.970	0.978	0.990	0.982
RMSE (kN)	610.203	588.446	263.932	278.495	359.464	310.513	196.297	485.172
MAPE (%)	22.7	20.6	8.8	7.6	11.4	10.9	7.4	17.7

Table 5 – Performance metrics of design methods for slender columns

Statistical parameters	AISC	GB	EC4	Uenaka	Hassanein	Han	Castanheira
$P_{n,exp}/ P_{n,pred}$ – Mean	0.71	0.62	0.56	0.59	0.64	0.63	0.72
$P_{n,exp}/ P_{n,pred}$ – Maximum value	0.84	0.73	0.65	0.67	0.73	0.72	0.82
$P_{n,exp}/ P_{n,pred}$ – Minimum value	0.64	0.53	0.50	0.54	0.59	0.58	0.63
$P_{n,exp}/ P_{n,pred}$ – Standard deviation	0.09	0.09	0.06	0.05	0.06	0.06	0.09
$P_{n,exp}/ P_{n,pred}$ – Coefficient of variation (%)	12.52	13.91	10.46	8.88	9.96	9.41	12.50
R^2	0.99	0.99	0.99	0.99	0.99	0.99	0.46
RMSE (kN)	943.51	1432.18	1557.89	1387.08	1174.16	1172.64	595.86
MAPE (%)	0.42	0.64	0.79	0.70	0.58	0.59	0.40

Fig. 3(a) and Fig. 3(b) show the accuracy of the formulations for short columns found in design codes and in the literature, respectively, presented together. It can be observed that the formulations proposed by the authors generally provide a better fit than those found in the evaluated codes. While Fig. 3(a) indicates an overestimation of up to 77.8%, the greatest overestimation among the formulations proposed by the authors is approximately half that value. Therefore, it can be noted that the formulations from the literature, in general, are closer to the red line.

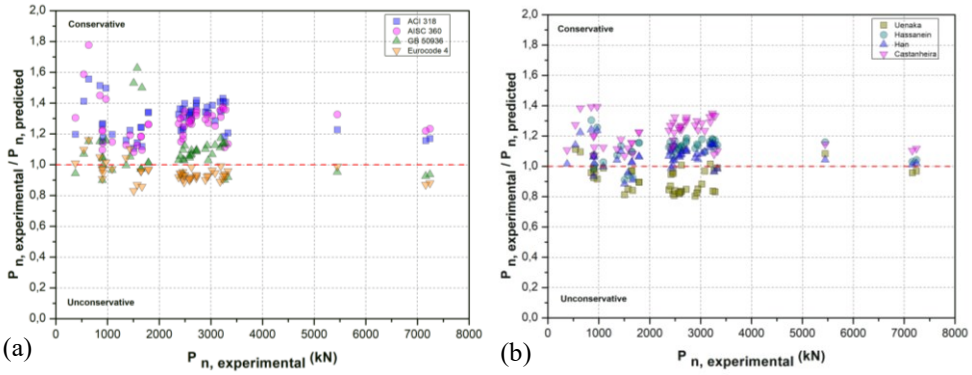

Figure 3 – The accuracy of the short double-skin columns resistance prediction: (a) standards; (b) literature.

Unlike short double-skin columns, all formulations exhibit unsatisfactory performance when applied to slender columns, as can be seen in Fig. 4. Slender CFDST columns are more prone to global buckling, reducing their load capacity. This occurs because, in slender columns, the load-bearing capacity is governed by second-order effects, in which the lateral displacements produced by axial loading increase the internal bending moments, intensifying instability. In addition, slender columns are highly sensitive to geometric imperfections and load

application eccentricities. Therefore, global instability leads to buckling and significantly reduces the load-carrying capacity of slender columns compared to short columns. Yet, most design methods are based on studies of short columns, limiting their accuracy for slender ones. This underscores the need for further research.

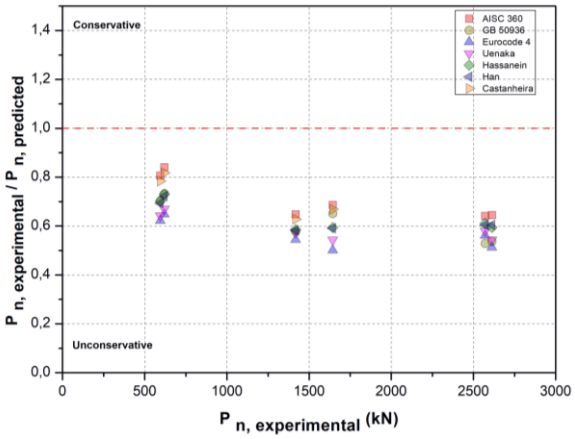

Figure 4 – The accuracy of the slender double-skin columns resistance prediction

4 Conclusions

This study presented the main existing design methods for CFDST columns and evaluated their respective accuracy. Among the design methods addressed in this study are the ACI 318: 2011 [3], AISC 360: 2016 [4], GB 50936: 2014 [5], and Eurocode 4: 2004 [6] standards, as well as formulations proposed by Uenaka et al. (2010) [7], Hassanein et al. (2013) [8], Han et al. (2018) [9], and Castanheira (2021) [10]. To verify the accuracy, performance metrics were calculated for each design method, including the Coefficient of Determination (R^2), Root Mean Square Error ($RMSE$), and Mean Absolute Percentage Error ($MAPE$). As shown in Fig. 2(b), the formulations proposed in the literature for short double-skin columns generally tend to perform more accurately compared to the design code formulations, as illustrated in Fig. 3. For short columns, the formulation proposed by Han et al. (2018) [9] proved to be the most accurate, presenting more satisfactory $R^2, RMSE$, and $MAPE$ values compared to the other formulations. In contrast, ACI 318:2011 [3] showed low accuracy and was overly conservative in its predictions

In contrast to short columns, the accuracy of the design methods for slender columns was unsatisfactory for all formulations. Except for the formulation proposed by Castanheira (2021) [10], all other formulations exhibited $RMSE$ values above 900 kN, which is considered high given that the dataset has an average ultimate axial load of 2324.27 kN. However, the formulation by Castanheira (2021) [10] showed a low R^2 value of 0.46. Additionally, all design methods presented $MAPE$ values above 40%

Therefore, the present study concluded that the design methods show satisfactory accuracy for short double-skin columns, especially the formulation proposed by Han et al. (2018) [9]. However, the equations demonstrated low accuracy when applied to slender double-skin columns. In this context, there is a clear need for further investigation into slender double-skin columns in order to accurately represent the effect of slenderness on their load-bearing capacity.

Acknowledgements. The authors gratefully acknowledge the financial support of CAPES (Coordination for the Improvement of Higher Education Personnel).

Authorship statement. The authors hereby confirm that they are the sole liable persons responsible for the authorship of this work, and that all material that has been herein included as part of the present paper is either the property (and authorship) of the authors, or has the permission of the owners to be included here.

References

[1] Lima, P. R. L.; Amiri, M. M.; Shadman, M.; Junkaic, F.; Estefen, A. F.; Filho, R. D. T. "Potencialidade de aplicação de UHPC em estruturas mistas para geração de energia eólica." In: Congresso Brasileiro de Estruturas Mistas (CBEM), 1., 2024, Maringá. *Anais do I congresso brasileiro de estruturas mistas. Maringá*: Universidade Estadual de Maringá, 2024, p. 318-327.
[2] Gonçalves, I. T.; Pereira, F. L. G.; Rodrigues, M. C.; Ribeiro, D. M.; De Lima, L. R. O. "Investigação de colunas tipo double-skin preenchidas com concreto." In: Congresso Brasileiro de Estruturas Mistas (CBEM), 1., 2024, Maringá. *Anais do I congresso brasileiro de estruturas mistas*. Maringá: Universidade Estadual de Maringá, 2024, p. 394-401.
[3] American Concrete Institute. *ACI 318-11*: Building code requirements for structural concrete and commentary. Farmington Hills, MI: ACI, 2011.
[4] American Institute Of Steel Construction. *ANSI/AISC 360-16*: Specification for structural steel buildings. Chicago, IL: AISC, 2016.
[5] China. Technical code for concrete filled steel tubular structures. Beijing: Ministry of Housing and Urban-Rural Development of the People's Republic of China, *GB 50936-2014*, 2014.
[6] European Committee For Standardization. Design of composite steel and concrete structures – Part 1-1: General rules and rules for buildings (*Eurocode 4*). Brussels, 2004.
[7] Uenaka, K.; Kitoh, H.; Sonoda, K. "Concrete filled double skin circular stub columns under compression." *Thin-Walled Structures,* v. 48, p. 19-24, 2010. DOI: http://dx.doi.org/10.1016/j.tws.2009.08.001
[8] Hassanein, M. F.; Kharoob, O. F.; Liang, Q. Q. "Circular concrete-filled double-skin tubular short columns with external stainless steel tubes under axial compression." *Thin-Walled Structures*, v. 73, p. 252-263, 2013. DOI: http://dx.doi.org/10.1016/j.tws.2013.08.017
[9] Han, L. H.; Lam, D.; Nethercot, D. "Design Guide for Concrete-filled Double Skin Steel Tubular Structures." 1 ed. London, *Taylor & Francis Group*, 2018. DOI: https://doi.org/10.1201/9780429440410
[10] Castanheira, Deborah Sousa. "Behaviour of concrete-filled double-skin stub columns with recycled aggregate concrete subjected to concentric and eccentric load." 2021. *Tese (Doutorado)* – Faculdade de Engenharia, Universidade do Estado do Rio de Janeiro, Rio de Janeiro, 2021.
[11] Tao, Z.; Han, L. H.; Zhao, X. L. "Behaviour of concrete-filled double skin (CHS inner and CHS outer) steel tubular stub columns and beam-columns." *Journal of Constructional Steel Research*, v. 60, n. 8, p. 1129–1155, 2004. DOI: http://dx.doi.org/10.1016/j.jcsr.2003.11.008
[12] Li, W.; Ren, Q. X.; Han, L. H.; Zhao, X. L. "Behaviour of tapered concrete-filled double skin steel tubular (CFDST) stub columns." *Thin-Walled Structures*, v. 57, p. 37–48, 2012.
[13] Li, W.; Cai, Y.-X. "Performance of CFDST stub columns using high-strength steel subjected to axial compression." *Thin-Walled Structures*, v. 141, p. 411–422, 2019. DOI: http://dx.doi.org/10.1016/j.tws.2019.04.021
[14] Ekmekyapar, T.; Hasan, H. G. "The influence of the inner steel tube on the compression behaviour of the concrete filled double skin steel tube (CFDST) columns." *Marine Structures*, v. 66, p. 197–212, 2019. DOI: http://dx.doi.org/10.1016/j.marstruc.2019.04.006